

## Numerical Simulation of Rigid Wheel Running Behavior on Sand Terrain

\*Mengyan Zang<sup>1</sup>, Chunlai Zhao<sup>1</sup>

<sup>1</sup>School of Mechanical & Automotive Engineering, South China University of Technology, Guangzhou, Guangdong  
510640

\*Corresponding author: myzang@scut.edu.cn

### Abstract

The 3D discrete element method (DEM) and finite element method (FEM) were combined together to investigate the running behavior of rigid wheel on sand terrain. Firstly, an efficient method for the initial generation of discrete elements (DEs) which is suitable for the simulation of sand terrain was introduced. Then, the DEs were consolidated to a steady state to model the real condition of sand terrain. Afterwards, a 3D numerical model was established based on the soil bin experiment to model the running behaviour of the rigid wheel travelling from hard terrain to sand terrain, where the wheel, the hard terrain and the soil bin were solved by using FEM. Finally, a constant angular velocity and corresponding translational velocity were loaded to the rigid wheel to investigate its running behavior under different slip ratios. Corresponding running behavior parameters like net draw bar pull and sinkage were obtained. The overall trend of net draw bar pull versus slip ratio is qualitatively in agreement with current experimental results.

**Keywords:** DEM; FEM; running behavior; sand terrain; rigid wheel

### 1 Introduction

Off-road vehicles, which have been widely used in agricultural production, planetary exploration, and military field, usually work on discontinuous granular road such as sand terrain. The deformation and destruction of the soft road have large effects on the traction performance of vehicles. Thus, the research of the wheel-road system interactions is significant to the parameter match and design of off-road vehicles. Many researchers (Robert, Winnie and Tim 2005; Yang, Xu, Liang, Zhang, et al, 2011; Maciejewski and Jarzebowski, 2004; Hisanori, Nakashima, Takatsu, et al, 2010) had been working on this filed via experimental methods, but these methods have shortcomings like long development time and expensive cost. Recently, with the rapid development of computer technology, simulation methods had been widely used in the research of this filed.

Finite element method (FEM) as a traditional simulation method has been used by many researchers. And many achievements have been reported in various literatures. For example, in order to simulate the deformation behavior of soft terrain under a rolling wheel, Hiroma, Wanjii, Kataoka, et al (1998) regarded the soft soil as viscoelastic material; LIU and Wong (1996) implemented a modified critical state model in conjunction with a new nonlinear elastic law into the general purpose finite element program MARC; Xia (2011), Xia and Yang, (2012) took the soil as elastoplastic material and implemented the Drucker-Prager/Cap model into ABQUS as a user subroutine. Moreover, Hambleton and Drescher (2008 and 2009) analyzed the running behavior of the rigid wheel travels from hard terrain to soft terrain, where the two kinds of road were modeled by elastoplastic material with different material parameters. Although these studies used different materials to model the soft terrain, the traditional FEM technology is unable to describe the discontinuous features of granular materials such as sand terrain with sufficient accuracy. Moreover, the effect of the tread pattern on traction performance is also unable to be described clearly by FEM.

On the contrary, the discrete element method (DEM) shows a clear advantage to handle such problems. For example, Lav, Vilas, Salokhe, et al (2007) applied DEM to the investigation of the running performance of smooth rigid wheel rolling on coarse sand and medium sand under different vertical load conditions, Nakashima, Fujii, Oida, et al (2007 and 2010) and Li, Huang, Cui, et al

(2010) investigated the running behavior between lugged wheel and lunar regolith via 2D DEM. For further research, Zhang, Liu, Zeng, et al (2012), Knuth, Johnson, Hopkins, et al (2012) used 3D DEM to analyze the interaction between planet rover wheels and martain terrain. However, in these studies, the wheels, wheel lugs and granular terrain were all modeled by DEM, therefore, the deformation and the complex tread pattern structure of the tire could not be simulated reasonably.

Nakashima and Oida (2004), Nakashima, Takatsu, Shinone (2009) and Nakashima, Takatsu (2008) used the 2D finite element and discrete element method (FE-DEM) to investigate the wheel traction performance on sand terrain, where the rigid wheel was discretized by FEs and the sand terrain was modeled via DEs. This method compensated for the demerits of the two methods. However, it is obvious that the complex behaviors such as lateral force and steering performance of a rolling wheel are unable to be described by the current 2D method.

The purpose of this study is to apply 3D FE-DEM to the investigation of the wheel traction performance on sand terrain. Related program code is developed based on FORTRAN95 language. The numerical model of rigid wheel rolling from hard terrain to soft sand terrain is established based on the soil bin experiment, where the wheel, hard terrain and soil bin are all discretized by FEM, the sand terrain is modeled by DEM. The running behaviors of the rigid wheel under different slip ratios are analyzed.

This paper is organized as follows: in the next section, the basic equations of FE-DEM, including the motion equations of elements and the interaction forces among elements are introduced. The concept of analysis for the wheel-sand interaction in FE-DEM is also illustrated. Sect.3 illustrates an efficient way for the initial generation of the DEs which is suitable for sand simulation and the consolidation process of the DEs under self-weight is also shown. Sect. 4 presents the numerical model of the wheel-sand interaction system. The traveling process of the wheel under different slip ratios is modeled. And corresponding results are also illustrated and analyzed in this section.

## 2. The FE-DEM algorithm introduced

### 2.1 Equations of motion

For the 3D FE-DEM algorithm, the motions of the DEs and FEs are governed by the second Newton's law. For arbitrary element  $i$ , the equations are expressed by Eq. (1) (used for both DEs and FEs) and Eq. (2) (only used for DEs).

$$m_i(d^2\mathbf{u}_i / dt^2) = \mathbf{F}_i \quad (1)$$

$$I_i(d^2\boldsymbol{\theta}_i / dt^2) = \mathbf{M}_i \quad (2)$$

Where  $m_i$  and  $I_i$  are the mass and inertia moment of element  $i$ , respectively;  $\mathbf{u}_i$  and  $\boldsymbol{\theta}_i$  are the displacement and the rotation angle of element  $i$ , respectively;  $\mathbf{F}_i$  and  $\mathbf{M}_i$  are the total external force and centroidal moment of element  $i$ , respectively.

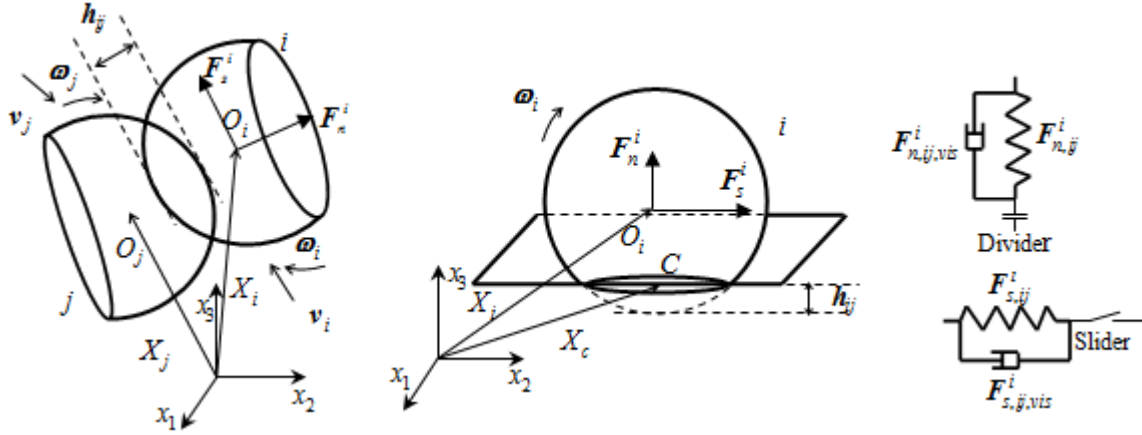
### 2.2 Interactions among elements and the wheel-sand system

Contact detection is the prerequisite for the calculation of interaction forces among elements. In this study, the C-grid detection method proposed by Williams, Perkins and Cook (2004) is used for DEs, and contact algorithm between 3D DEs and FEs has been previously developed by the authors (Zang, Gao, Lei, 2011). The contact models for elements are shown in Fig. 1. Where  $h_{ij}$  is the overlap of contacting elements;  $\mathbf{v}_i, \mathbf{v}_j, \boldsymbol{\omega}_i, \boldsymbol{\omega}_j$  are the velocity and angular velocity of element  $i$  and  $j$ , respectively;  $F_n^i$  is the normal force, and  $F_s^i$ , taken Coulomb friction law into account, is the tangential force of element  $i$ , which can be obtained from Eq. (3) and Eq. (4).

$$\mathbf{F}_n^i = \mathbf{F}_{n,ij}^i + \mathbf{F}_{n,ij,vis}^i \quad (3)$$

$$F_s^i = \begin{cases} F_{s,ij}^i + F_{s,ij,vis}^i & |F_s^i| < |F_n^i| \mu \\ F_n^i \mu & |F_s^i| \geq |F_n^i| \mu \end{cases} \quad (4)$$

Where  $F_{n,ij}^i$ ,  $F_{n,ij,vis}^i$ ,  $F_{s,ij}^i$ , and  $F_{s,ij,vis}^i$  are the normal spring force, the normal damping force, the tangential spring force and the tangential damping force of element  $i$ , respectively; These forces can be calculated via Hertz theory and Mindlin theory (Robertas, Algis, Rimantas, 2004);  $\mu$  is the friction coefficient. It should be noted that the FE was regarded as sphere with infinite radius (Han and Owen, 2000) when calculate the interaction force between FE and DE as illustrated in Fig. 1(b).



(a) Contact between DE and DE (b) Contact between FE and DE (c) Force between elements  
**Fig. 1 Contact models among elements**

Based on the theory mentioned above, the concept of analysis for the wheel-sand interaction by FE-DEM is illustrated in Fig. 2. The interactions among sand particles are solved via interactions of DEs (Fig. 1(a)), while the forces between tire and sand particles are calculated by interactions between FE and DE (Fig. 1(b)).

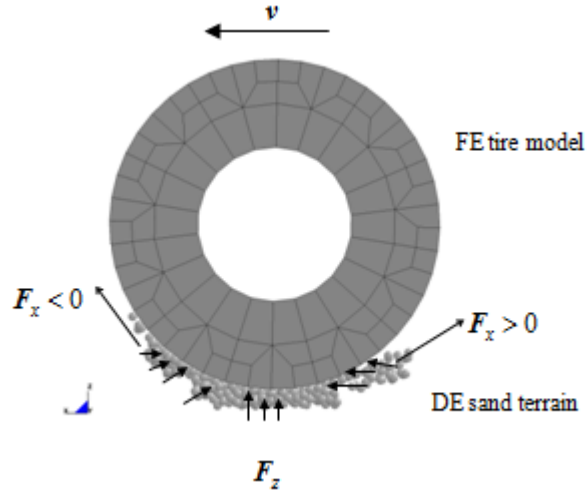


**Fig. 2 Description of wheel-sand system by FE-DEM**

The net draw bar pull  $N$ , normal reaction force  $P$  and slip ratio  $s$  are defined as follows:

$$N = G - |R| \quad (5)$$

$$P = \sum F_z \quad (6)$$

$$s = (1 - v / (r\omega)) \quad (7)$$

Where  $F$  is the contact force between FE wheel and DE terrain;  $G = \sum F_x^+$  and  $R = \sum F_x^-$  are the gross traction force and the resistance force, respectively;  $v$  and  $\omega$  are the translational speed and the angular velocity of the wheel;  $r$  is the free rolling radius of wheel.

### 2.3 Program flow

The simulation of the wheel running process is composed of following three steps: Step1, granular DEs compact to a steady state under self-weight; Step2, the FE wheel sink onto the FE road surface under vertical load including self-weight and external load until it reaches an equilibrium state; Step3, a constant angular velocity and corresponding translational velocities are loaded to the wheel center to analyze its traction performance under various slip ratios. And the wheel travels from FE hard road to DE soft terrain. The program flow chart is shown in Fig. 3.

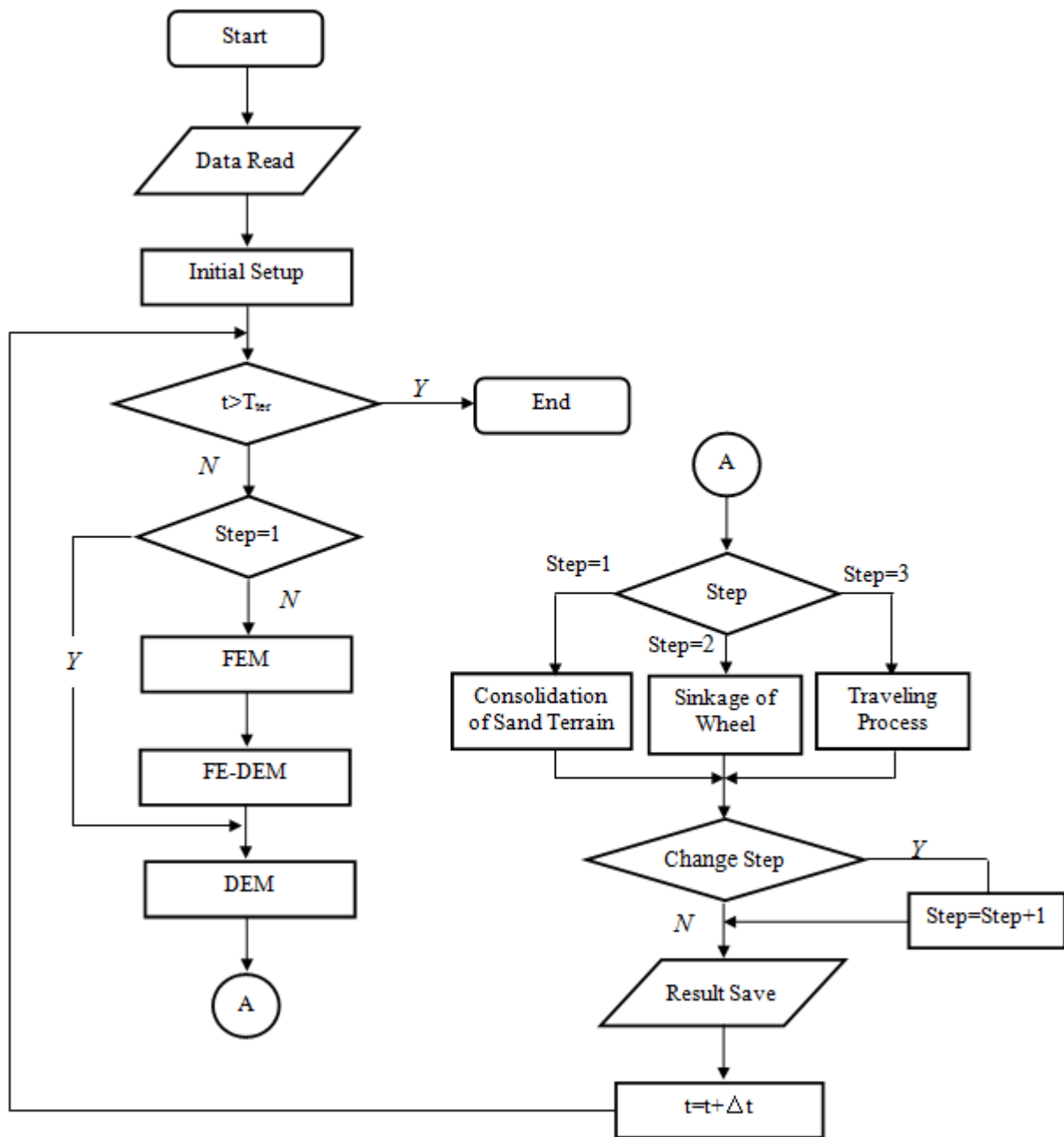


Fig. 3 Program flow chart

### 3 DE modeling of soft sand terrain

#### 3.1 Initial generation

The discontinuous characteristics of loose gravel terrain can be modeled effectively by DEM (Fujii, et al, 2010; Li, et al, 2010; Zhang, et al, 2012; Knuth, et al, 2012; Nakashima, et al, 2004 and Nakashima, et al 2009). Thus, we use the 3D DEM to model the sand terrain in this paper. The initial generation of the DEs is one of the main research topics. For this problem, Han, Feng, Owen (2005) proposed a method for the generation of spheres which randomly distributed in a given geometric domain with different sizes. The details are as follows:

1. Various sizes of spheres which are randomly distributed in a given geometric domain are generated, and there are gaps among spheres.
2. Find out the neighbor spheres of each sphere. Calculate the distance between the target sphere and its neighbor spheres in a given direction (in this study is the vertical direction), and move the target sphere to the nearest neighbor sphere along the special direction, the moving distance is equal to the minimum distance.
3. Further compression is executed similar to step2 to improve the volume density of the spheres, where the compression direction  $V_l = \alpha V_g + \beta V_n$ , as illustrated in Fig. 4, changes in a given range.

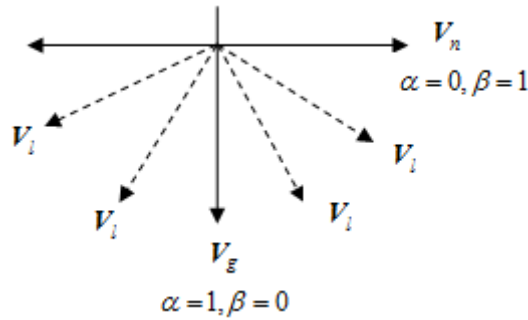


**Fig. 4 Compression directions**

After the above steps are completed, a void will be produced on the upper part of the domain. In order to fill the void, a strategy of sphere insertion was adopted by Han, et al (2005): spheres were generated at the top of the domain and then dropped along the compression direction until they contact with the nearest existing sphere. During this procedure, it needs to loop over all the current spheres for the contact detection, which wastes a lot of computing time. With the increasing of the sphere number, the consumption of the computing resource is increased dramatically. For the sand terrain simulation problem, large amount of spheres need to be generated. What's more, considering that the spheres should be consolidated under self-weight to a steady state to model the real sand condition after the initial generation, we prefer the improving of efficiency to the increasing of volume density at the initial generate stage.

Hierarchical generative method is applied to enhance the efficiency of the initial generation in this study. A 2D schematic diagram is shown in Fig. 5. Firstly, various sizes of spheres are generated in a given geometric domain as illustrated in Fig. 5(a). Then, the spheres are compressed by using the method of Han, et al (2005), a new terrain A is created as shown in Fig. 5(b). Afterward, new spheres are generated and compressed in the new terrain A, as shown in Fig. 5(c), Fig. 5(d). Another new terrain A is produced as illustrate in Fig. 5(d). Repeat the above procedure until no sphere of given radius range can be generated. In this procedure, the contact detection only needs to be executed among spheres in the new domain A for every layer of generation.

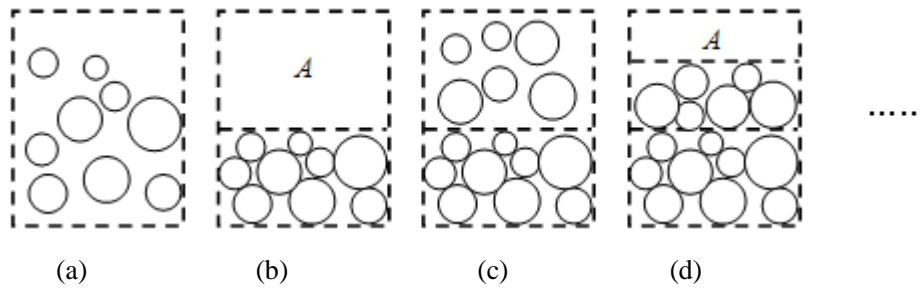


**Fig. 5 Hierarchical generate method**

In order to validate the superiority of the new method, a given number of spheres were generated in special geometric domains via hierarchical method and the method of Han, et al (2005), the results are shown in Fig. 6. It can be seen that the former method is more efficient than the latter one when generate same amount of spheres in a given geometric domain. With the increase of the computing scale, the efficiency is improved more significantly. For the geometric domain of  $2000 \times 640 \times 380$ mm and sphere number of 170000, the calculation efficiency can be improved by 60%.

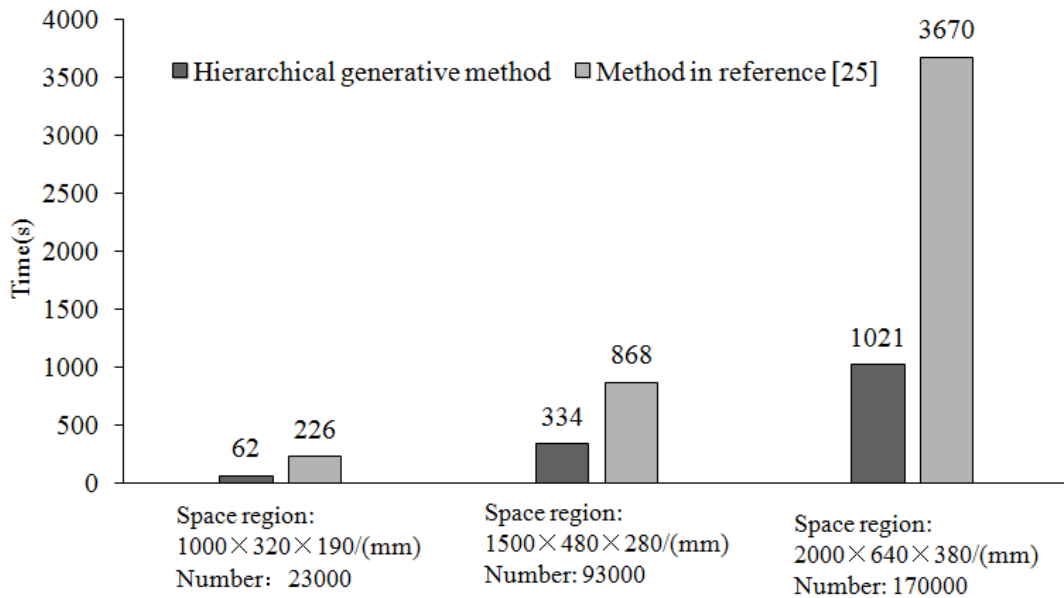


**Fig. 6 Comparing of the computation time**

The initial configuration of the sphere DEs in the geometric domain of  $1500 \times 480 \times 280$ mm with sphere number of 93024 is shown in Fig. 7.

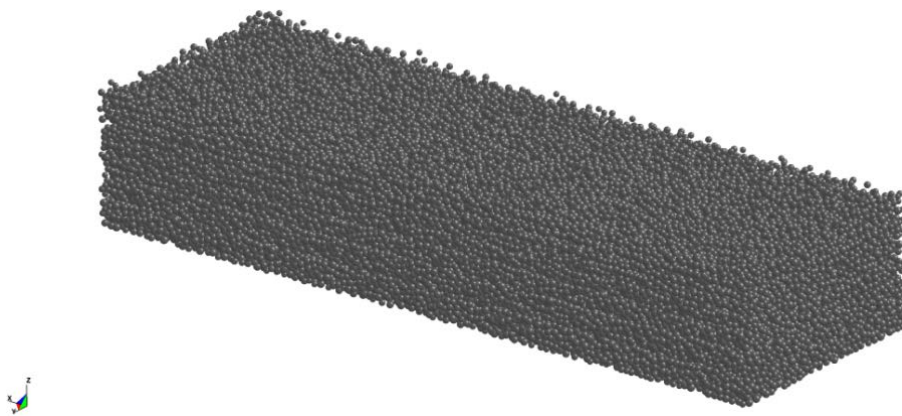


**Fig. 7 Initial configuration of the DEs in geometric domain of  $1500 \times 480 \times 280$ mm**

### 3.2 DEs consolidation under self-weight

It should be noticed that there might be contact but no contact force among DEs after initial generation. This is different with the real state of the sand particles. Therefore, the DEs shown in Fig. 7 were placed into the soil bin with corresponding geometric size. Then, gravitational force was loaded to the DEs, and they were compacted to a stable state under self-weight. The displacement nephogram of the vertical direction during the compaction procedure is shown in Fig. 8. It can be seen that the displacements of the elements in the bottom of the soil bin are small, while the elements in the upper part of the soil bin show larger displacements.

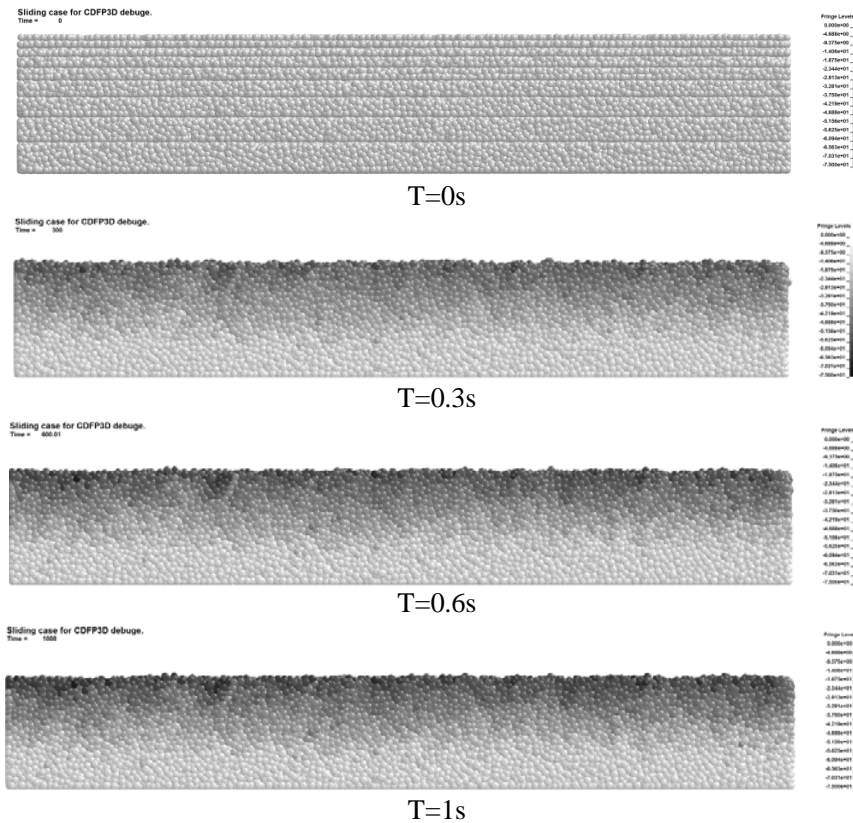


**Fig. 8** Displacement nephogram of vertical direction of DEs during consolidation process

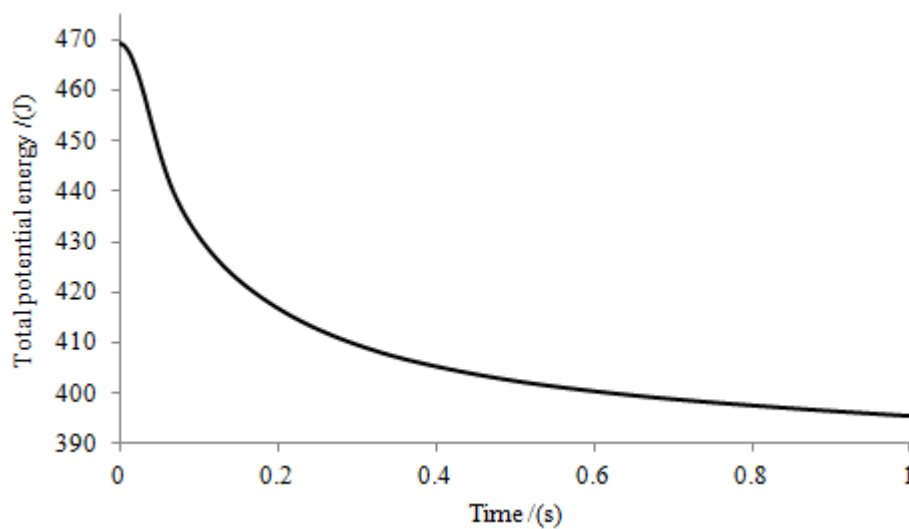


**Fig. 9** Time history of total potential energy of DEs

Total gravitational potential energy is used to estimate the consolidation state, and the time history of the total gravitational potential energy is illustrated in Fig. 9. It is obvious that the total potential energy decreases with the increasing of the computing time, and the trend tends to be flat. After 1s of consolidation, it tends to be stable, and the consolidation process is completed.

#### 4 Numerical simulation of running behavior

##### 4.1 Model introduced

Based on the soil bin experiment by Hisanori, et al (2010), considering that the wheel usually travels from hard terrain into soft terrain in practice, refer to papers of Hambleton, et al (2008 and 2009), the numerical model is established including hard terrain and soft terrain, as illustrated in Fig. 10, where the hard terrain, wheel and soil bin are discretized by FEs. The soft sand terrain is modeled by DEs with the geometric terrain of  $1500 \times 480 \times 280\text{mm}$  as illustrated in Fig7, and corresponding self-weight consolidation process is shown in Fig. 8, Fig. 9.

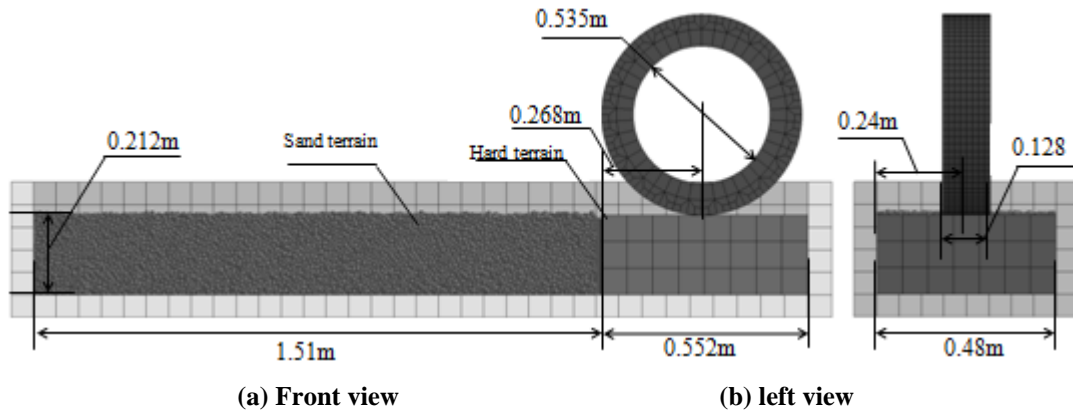


**Fig. 10 3D numerical model**

It should be noticed that we are focusing on the development 3D FE-DEM program in this paper, thus, the destruction of the tire, hard terrain and soil bin is neglected. The hard terrain and soil bin are modeled via elastic material. The radius range of the DEs is 5mm to 7mm. Time step for explicit calculation is  $10^{-5}\text{s}$ . Other parameters of the model are shown in Table1 and Table 2.

**Table 1 Material parameters**

	Wheel	Soil Bin	Hard Terrain	Sand Terrain
Number of Elements	1344	800	168	93024
Yong's Modulus (MPa)	2	$7.5 \times 10^4$	$7.5 \times 10^4$	$7.5 \times 10^4$
Poisson's Ratio	0.49	0.30	0.30	0.30
Density ( $\text{kg/m}^3$ )	$1.8 \times 10^3$	$2.4 \times 10^3$	$2.4 \times 10^3$	$2.4 \times 10^3$

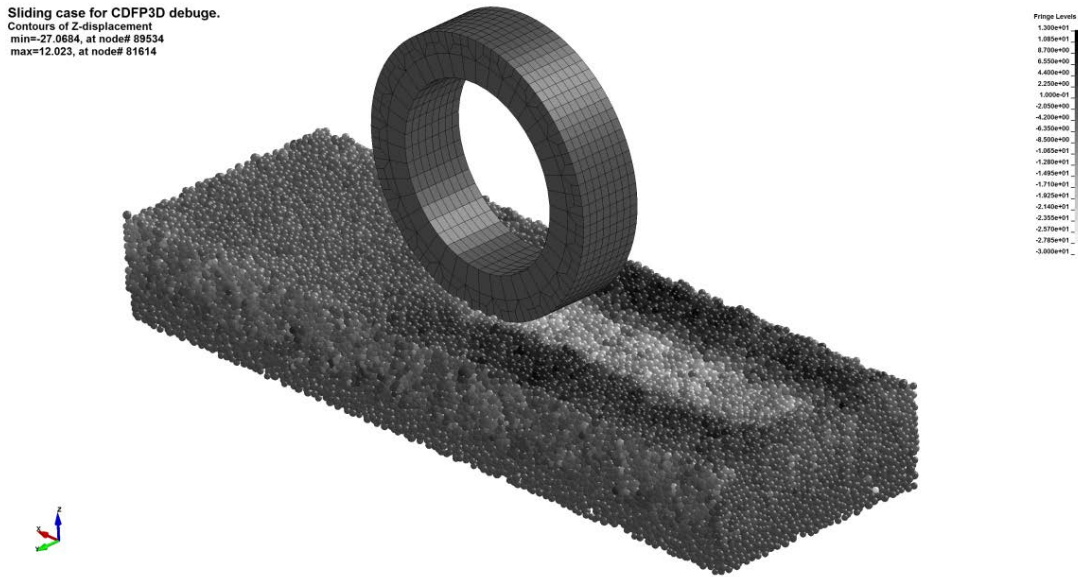
**Table 2 Contact parameters**

	Wheel-Sand	Wheel-Hard terrain	Soil-Bin
Normal Damping Coefficient (1/s)	40	50	50
Tangential Damping Coefficient (1/s)	35	45	45
Friction Coefficient	0.4	0.3	0.3

##### 4.2 The wheel traveling process

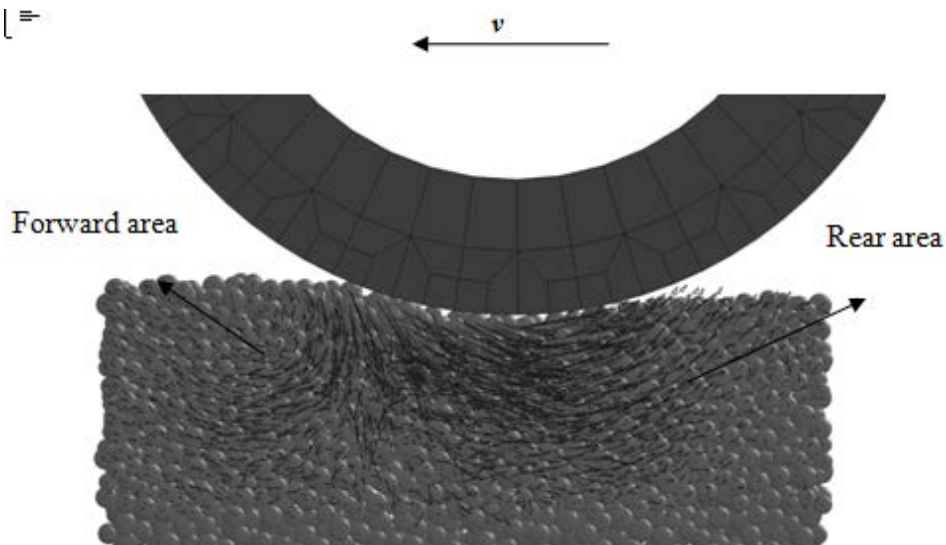
Firstly, according to the relevant experiment of Kyoto University (Hisanori, et al, 2010), vertical load of 1295N including self-weight and external load is loaded to the center of the wheel, and the wheel is sinking until reaches equilibrium state. Then, a constant angular velocity of 5rad/s and corresponding translational velocity are enforced to the center of the wheel to simulate its running

behavior under slip ratio of 30%. It should be noticed that the constant angular velocity value is set to 5rad/s, which is larger than that in Hisanori's experiment, to reduce the running time of the wheel for a certain traveling distance because of the low computational efficiency of the program. And the improvement of the computational efficiency is our future work. The displacement nephogram of Z direction of the DEs is shown in Fig. 11. For better observation, the soil bin and the hard terrain is not shown. The figure shows that for the elements under the wheel track, with light color, the displacement values are negative, while on both sides of the trace, with dark color, the displacement values are positive. This phenomenon is consistent with the real condition.



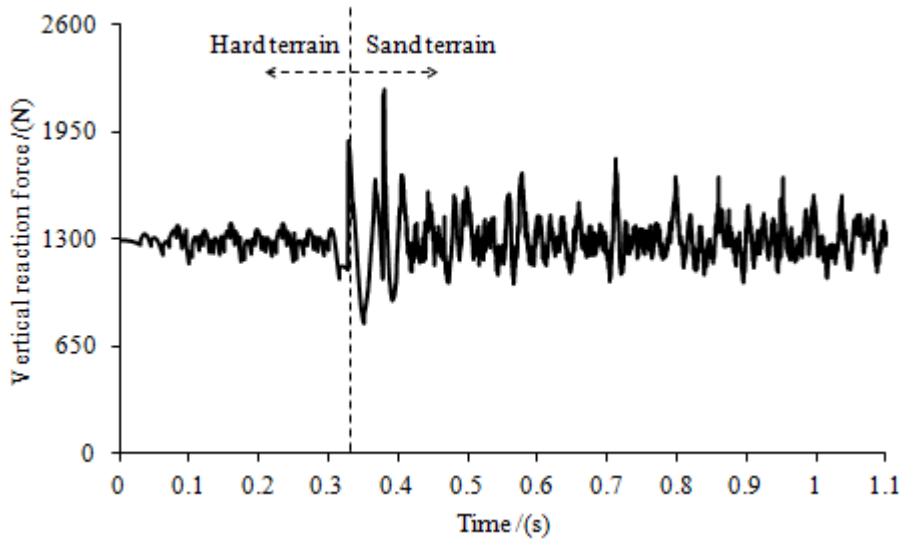
**Fig. 11 Displacement nephogram of Z direction of sand particles**

The flow of the sand particles has a great influence on running behavior of the wheel. Fig. 12 shows the flow trend of the particles at 0.74s, where the flow directions are described via velocity vectors. From the figure we can see that the flow trend of the particles can be divided into two areas, the forward flow in clockwise and the rear flow in anticlockwise. This phenomenon is consistent with the conclusions by Hambleton, et al (2009) and Zhuang (2002).



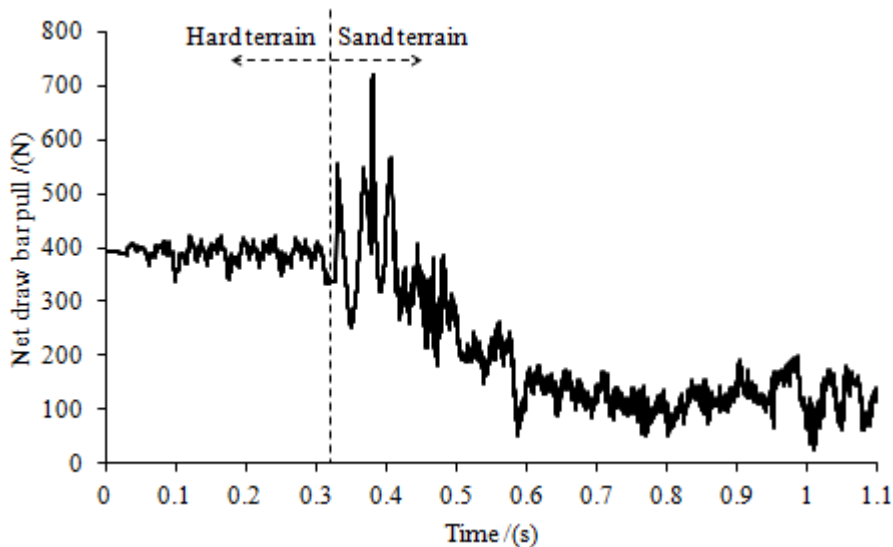
**Fig. 12 Configuration of sand flow trend**

Fig. 13 shows the time history of the vertical reaction force during the traveling process. It can be seen that the vertical reaction force fluctuates around the average value of 1300N, which is close to the given load value. The vertical reaction force on the soft sand terrain shows larger fluctuation than that on the hard terrain. The wheel starts to travel into the sand terrain at about 0.33s, and the vertical reaction force shows an abrupt fluctuation. The possible reason for this phenomenon is because of the sudden change of the support capacity of the road, the wheel sinks suddenly and the impact force leads to the fluctuation of the vertical reaction force.



**Fig. 13 Time history of the vertical reaction force**

The time history of the net drawbar pull is shown in Fig. 14. It can be seen that the net draw bar pull on the hard terrain is larger than that on the soft sand terrain. As the wheel travels into the sand terrain after 0.33s, the average value of the net draw bar pull decreases dramatically from 380N to 110N. Analogous to the vertical reaction force shown in Fig. 13, the net draw bar pull of the soft sand terrain shows a larger fluctuation than that on the hard terrain. Similar mutation at the conjunction of two kinds of roads is also illustrated in the figure.



**Fig. 14 Time history of net draw bar pull**

Fig. 15 shows the time history of the wheel sinkage. It can be seen that the wheel sinkage fluctuate in a small range on the hard road. As the wheel travels into the soft sand terrain after 0.33s, the

sinkage value increases dramatically because of the destruction of the terrain. Afterward, the trend tends to be flat and the value fluctuates in 24mm to 28mm.

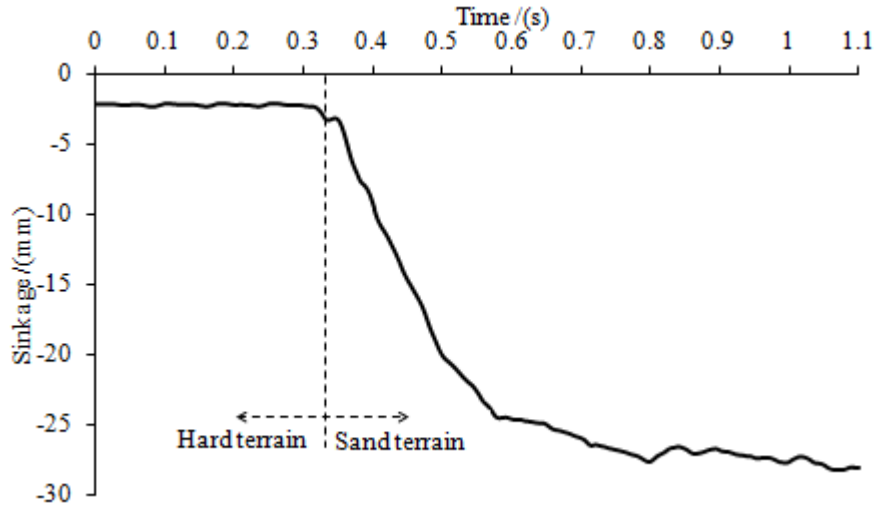


**Fig. 15 Time history of wheel sinkage**

In order to further analyze the effect of slip ratio on the running behavior of the wheel on sand terrain (net draw bar pull of hard terrain is not included), constant angular velocity of 5rad/s and corresponding translational velocity for different slip ratios according to Eq.(7) are enforced to the center of it. The average value of the net draw bar pull on the soft sand terrain is regarded as the equivalent value. The relation between the equivalent value of net draw bar pull and slip ratio is shown in Fig. 16. It is clearly that the value of the net draw bar pull rises with the increase of the slip ratio. And the trend is steeper when the slip ratio is less than 25%, then it shows a flat trend with the slip ratio larger than 25%,

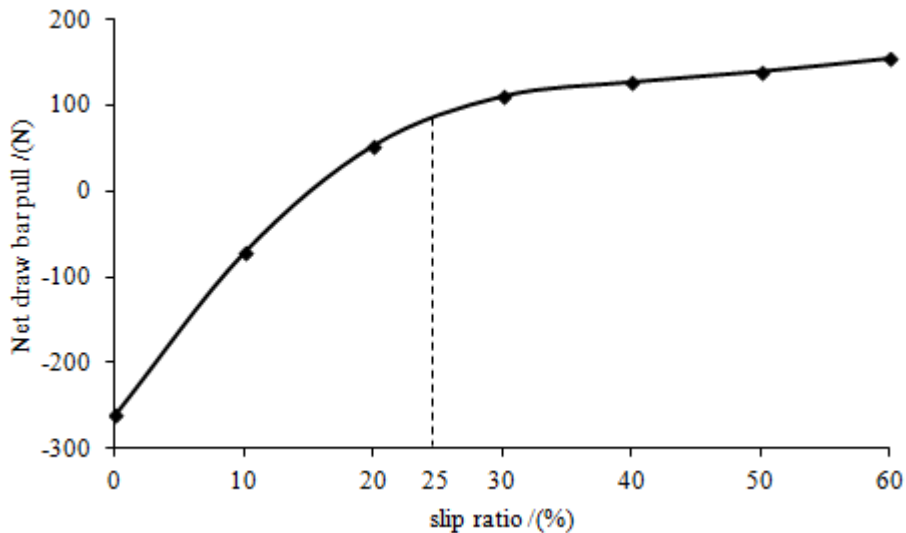


**Fig. 16 Relation between net draw bar pull and slip ratio**

Fig. 17 shows the sinkage of the wheel with the traveling distance of 0.4m on sand terrain (sinkage on hard terrain is not included) under different slip ratio values. It can be seen that the value of the sinkage rises with the increase of the traveling distance. The sinkage value also rises with the increase of the slip ratio, for slip ratio value of 0% and 60%, the maximum values of the sinkage are 17.8mm and 37.9mm, respectively.

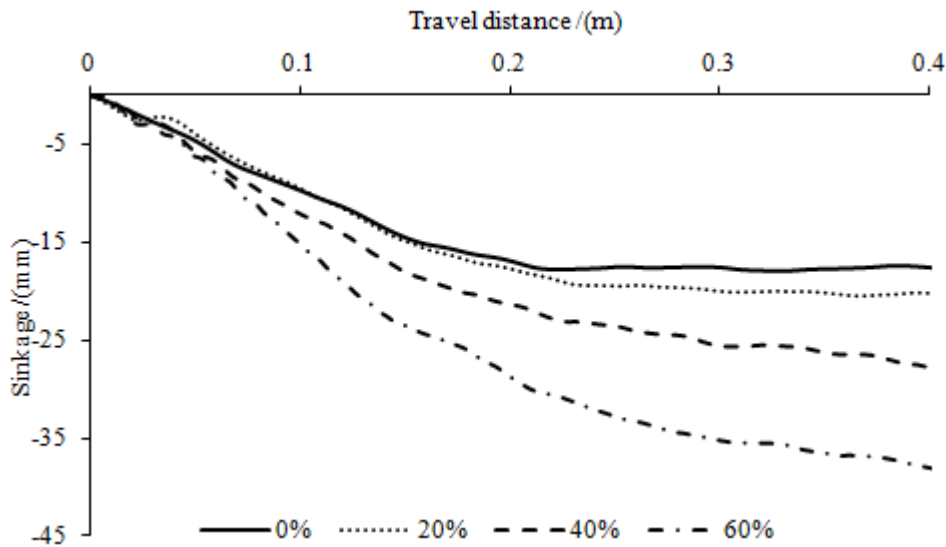


**Fig. 17 Relation between wheel sinkage and slip ratio**

#### 4.3 Simulation results discussion

From the above simulation, we can obtain the following results:

Hard terrain shows better traction performance than that of soft sand terrain, and the driving process is stable. During the process of running on sand terrain, the road is destructed, the net draw bar pull shows larger fluctuation, and the rut is clear. The main reason is because of the rolling and flow characters of the sand particles. Although we consider the frictions among DEs, the sphere shape of the elements is still inconsistent with the actual situation of sand particles. Various shape elements (Li, et al (2010), Chen, Zhao, Cui, et al (2012), Zhou, Hua, Ma, et al (2012)) and rolling resistance among elements (Iwashita, Oda (2000), Jiang, Yu, Harris (2006) ) will be considered in the future to improve current program.

As the wheel travels into soft sand terrain, the sinkage value increases dramatically. Meanwhile, the normal reaction force and the net draw bar pull show large fluctuations. The reason is because of the different support capacity between hard and sand terrain, this causes an unbalance force of the wheel in the vertical direction. Thus, the wheel sinks into the sand terrain and produces large impact force which leads to the fluctuation of vertical reaction force. Moreover, the average value of the traction force decreases gradually because of the rolling and flow of the sand particles.

On the soft sand terrain, the net draw bar pull shows a steeper trend when the slip ratio is less than 25%, and the trend is flat when the slip ratio is larger. With the same traveling distance, the sinkage value rises with the increase of the slip ratio. These conclusions agree qualitatively with the results proposed by Hisanori, et al (2010) and Li, et al (2010). In the mean time, there are still problems that the value of the net draw bar pull is larger than that in Hisanori's experimental results. The possible reason is because of the larger particle size and the larger angular velocity of the wheel. And this problem will be overcome after we develop the parallel computing program which can improve the computing efficiency.

#### 5 Conclusions

1. In this study, a 3D FE-DEM has been applied to model the interaction between wheel and sand, and corresponding procedure code was developed based on FORTRAN95 language.
2. An initial generation method named hierarchical generate method which was appropriate for the sand terrain simulation was developed. Corresponding numerical model was established to model the running behavior of the wheel travels from hard terrain to soft sand terrain. The time

history of normal reaction force, net draw bar pull and sinkage of the wheel were obtained. The damage of the sand terrain was also presented.

3. The overall trend of the net drawbar pull versus slip ratio is agreed qualitatively with the results of previous experiments, this indicates the effectiveness of the 3D FE-DEM in analysis the traction performance of rigid wheel travels on sand terrain.

Plans for the future work are to improve the accuracy and the efficiency of the method. The tread pattern will also be considered to simulate the real tire behavior.

## Acknowledge

This work was supported by the National Natural Science Foundation of China (NO. 10972079 and NO. 11172104) and The International Cooperation Project of the Ministry of Science and Technology of China (2013DFG60080).

## Reference

- Robert Bauer, Winnie Leung, Tim Barfoot (2005), Experimental and Simulation Results of wheel-soil interaction for planetary rovers. *IROS 2005*. PP. 586-591.
- Runhuai Yang, Min Xu, Xu Liang, Shiwu Zhang, et al. (2011), Experimental study and DEM analysis on rigid driving wheel's performance for off-road vehicles moving on loose soil. *ICMA 2011*. PP. 142-147.
- J. Maciejewski, A. Jarzebowski. (2004), Experimental analysis of soil deformation below a rolling rigid cylinder. *Journal of Terramechanics*, 41(4), PP. 223-241.
- Hisanori SHINONE, Hiroshi NAKASHIMA, Yuzuru TAKATSU, et al. (2010), Experimental Analysis of Tread Pattern Effects on Tire Tractive Performance on Sand using an Indoor Traction Measurement System with Forced-slip Mechanism. *Engineering in agriculture environment and food*, 3(2), pp. 61-66.
- T. Hiroma, S. Wanjii, T. Kataoka, et al. (1998), Stress analysis using FEM on stress distribution under a wheel considering friction with adhesion between a wheel and soil. *Journal of Terramechanics*, 34(4), pp. 225-233.
- Liu C H, Wong J Y. (1996), Numerical simulation of tire-soil interaction based on critical state soil mechanics. *Journal of Terramechanics*, 33(5), pp. 209-221.
- Kaiming Xia. (2011), Finite element modeling of tire/terrain interaction: Application to predicting soil compaction and tire mobility. *Journal of Terramechanics*, 48(2), pp.113-123.
- Kaiming Xia, Yunming Yang. (2012), Three-dimensional finite element modeling of tire/ground interaction. *International journal for numerical and analytical methods in geomechanics*, 36(4), pp. 498-516.
- J.P. Hambleton, A. Drescher. (2008), Modeling wheel-induced rutting in soils: Indentation. *Journal of Terramechanics*, 45(6), pp. 201-211.
- J.P. Hambleton, A. Drescher. (2009), Modeling wheel-induced rutting in soils: rolling. *Journal of Terramechanics*, 46(2), pp. 35-47.
- J.P. Hambleton, A. Drescher. (2009), On modeling a rolling wheel in the presence of plastic deformation as a three- or two-dimensional process. *International Journal of Mechanical Sciences*, 51(11-12), pp. 846-855.
- Lav R.Khot, Vilas M. Salokhe, H.P.W.Jayasuriya, et al. (2007), Experiment validation of distinct element simulation for dynamic wheel-soil interaction. *Journal of Terramechanics*, 12(44), pp. 429-437.
- H.Nakashima, H.Fujii, A.Oida, et al. (2007), Parametric analysis of lugged wheel performance for a lunar microrover by means of DEM. *Journal of Terramechanics*, 44(2), pp. 153-162.
- H.Nakashima, H.Fujii, A.Oida, et al. (2010), Discrete element method analysis of single wheel performance for a small lunar rover on sloped terrain. *Journal of Terramechanics*, 47(5), pp. 307-321.
- Wen Li, Yong Huang, Yi Cui, et al. (2010), Trafficability analysis of lunar mare terrain by means of the discrete element method for wheeled rover locomotion. *Journal of Terramechanics*, 47(3), pp. 161-172.
- Zhang Rui, Liu Fang, Zeng Gui-Yin, et al. (2012), Research on Dynamic Simulation System of Interactions between Irregular Rigid Wheel and Lunar Soil Simulant. *CMGM-2012*. pp. 438-443.
- M.A. Knuth, J.B. Johnson, M.A. Hopkins, et al. (2012), Discrete element modeling of a Mars Exploration Rover wheel in granular material. *Journal of Terramechanics*, 49(1), pp. 27-36.
- NAKASHIMA H, Oida A. (2004), Algorithm and implementation of soil-tire contact analysis code based on dynamic FE-DE method. *Journal of Terramechanics*, 41(2-3), pp. 127-137.
- Hiroshi NAKASHIMA, Yuzuru TAKATSU, Hisanori SHINONE. (2009), FE-DEM Analysis of the effect of tread pattern on the tractive performance of tires operating on sand. *Journal of mechanical systems for transportation and logistics*, 2(1), pp. 55-65.
- Hiroshi NAKASHIMA, Yuzuru TAKATSU. (2008), Analysis of tire tractive performance on deformable terrain by finite element-discrete element method. *Journal of computational science and technology*, 2(4), pp. 423-434.

- John R. Williams, Eric Perkins, Ben Cook. (2004), A contact algorithm for partitioning  $N$  arbitrary sized objects. *Engineering Computations*, 21(2/3/4), pp. 235-248.
- Zang MY, Gao W, Lei Z. (2011), A contact algorithm for 3D discrete and finite element contact problems based on penalty function method. *Computational Mechanics*, 48(5), pp. 541-550.
- Robertas Balevičius, Algis Džugys, Rimantas Kačianauskas. (2004), Discrete element method and its application to the analysis of penetration into granular media. *Journal of civil engineering and management*, 10(1), pp. 3-14.
- Han K, Perić, D.R.J. Owen. (2000), A combined finite/discrete element simulation of shot peening processes Part II: 3D interaction laws. *Engineering Computations*, 17(6), pp. 680-702.
- K. Han, Y.T. Feng, D.T.J. Owen. (2005), Sphere packing with a geometric based compression algorithm. *Powder Technology*, 155(1), pp. 33-41.
- ZHUANG Jide. (2002), Computational vehicle terramechanics. *China Machine Press*.
- Chen Youchuan, Zhao Yongzhi, Cui Zequn, et al. (2012), Study of Discrete Element Simulation of Non-Sphere Base on Superquadrics. CMGM-2012. pp. 76-85.
- Zhou Wei, Hua Jun-Jie, Ma Gang, et al. (2012), Study on Deformation Mechanism of Rockfill Dams during an Initial Impoundment Process. CMGM-2012. pp. 307-320.
- Kazuyoshi Iwashita, Masanobu Oda. (2000), Micro-deformation mechanism of shear banding process based on modified distinct element method. *Powder Technology*, 109(1-3). pp. 192-205.
- M. J. Jiang, H.S. Yu, D. Harris. (2006), Bond rolling resistance and its effect on yielding of bonded granulates by DEM analyses. *International Journal for Numerical and Analytical Methods in Geomechanics*, 30(8), pp. 723-761.